arXiv:1611.01173v1 [physics.flu-dyn] 3 Nov 2016

Vortex arrays and ciliary tangles underlie the feeding–swimming tradeoff in starfish larvae

William Gilpin[1], Vivek N. Prakash[2], Manu Prakash[2*]

[1]Department of Applied Physics, [2]Department of Bioengineering,

Stanford University, Stanford, CA

[*]To whom correspondence should be addressed; E-mail: manup@stanford.edu

November 7, 2016

Abstract

Many marine invertebrates have larval stages covered in linear arrays of beating cilia, which propel the animal while simultaneously entraining planktonic prey.[1] These bands are strongly conserved across taxa spanning four major superphyla,[2, 3] and they are responsible for the unusual morphologies of many invertebrates.[4, 5] However, few studies have investigated their underlying hydrodynamics.[1, 6] Here, we study the ciliary bands of starfish larvae, and discover a beautiful pattern of slowly-evolving vortices that surrounds the swimming animals. Closer inspection of the bands reveals unusual ciliary "tangles" analogous to topological defects that break-up and re-form as the animal adjusts its swimming stroke. Quantitative experiments and modeling suggest that these vortices create a physical tradeoff between feeding and swimming, which manifests as distinct flow patterns or "eigenstrokes" representing each behavior—potentially implicating neuronal control of cilia. This quantitative interplay between larval form and hydrodynamic function generalizes to other invertebrates, and demonstrates the potential of active boundary conditions in other biological and synthetic systems.

Many marine invertebrates develop in two stages, growing from swimming larvae to bottom-dwelling adults. This developmental dichotomy mandates physical tradeoffs, resulting in a stunning variety of larval morphologies that have transfixed biologists and artists alike for more than a century.[7] Common to many larval forms are dense ciliary bands encircling the body, which propel the animal during escape and dispersal while also entraining motile plankton, their primary food source.[1] Ciliary bands are very high density cilia aligned in linear arrays, which are as morphologically diverse as the remarkable range of organisms in which they appear (which spans four major superphyla).[3] Although several studies have emphasized the importance of ciliary bands in phylogenetic reconstruction,[2] few have quantitatively investigated them, particularly the physical mechanism by which they simultaneously maximize swimming flow while precisely capturing single food particles—an intrinsic link between larval morphology and behavior.

Here, we observe that the larva of the common starfish *Patiria miniata* generates around its body a beautiful and intricate array of counter-rotating vortices, which merge and split in a complex manner over time (Figure 1C, Supplementary Video 1; 29 larvae). We find these patterns in both freely-swimming and animals held stationary, and the larvae swim irregularly as these currents evolve (Supplementary Videos 2, 3, 4; 37 larvae). Slowly-varying recirculation currents have been noted in several marine larvae,[1, 4–6] and we hypothesize that these structures play a crucial role in resolving the requirements of both swimming and feeding. Here we investigate this conjecture using a combination of live imaging and mathematical modeling, and we reveal a subtle interplay between organism-level morphology and microscopic ciliary tangles, which jointly produce the distinctive, dynamic flow fields seen around the organism. We further analyze these flow fields in order to identify separate hydrodynamic "eigenstrokes" corresponding to distinct feeding and swimming behaviors. To our knowledge, our results provide the first quantitative study of the relationship between form and function in ciliary bands, and we suggest that the competing hydrodynamics of feeding and swimming may unify morphology and behavior in marine invertebrates.

Ciliary bands in a *Patiria miniata* larva surround the animal's periphery, dividing the body into pre- and post-oral hoods and the circumoral field, with most swimming occurring with the pre-oral hood facing forward (Fig. 1A).[1] The circumoral bands are primarily responsible for the observed vortices, which localize to the animal's midplane. The vortices remain mostly symmetric across the body axis (although this symmetry varies over time), and minor left-right differences in body morphology create small asymmetries in the vortex locations. The largest vortices occur at the posterior end of the larvae, while smaller vortices localize to dense portions of the band near the side lobes. Stagnation points with zero net flow form where two counter-rotating vortices intersect. Consistent with previous larval feeding experiments,[6, 8] algae that pass through the vortex field and contact the body surface are captured and then passed from cilium to cilium within the circumoral field until they reach the mouth, where they aggregate before being transported into the gut. An electron micrograph of a larvae reveals shorter cilia covering the body surface that facilitate this transfer, with higher line densities of cilia ($\sim$ 3 cilia/μm) occurring along the ciliary band than on the body surface ($\sim$ 0.5 cilia/μm) (Fig. 1B). This unusually high density and configuration of cilia enables physical interactions between neighboring cilia, an uncommon feature in single cell ciliates.[9, 10]

Closer inspection of the cilia reveals a typical stroke pattern (Fig. 2D) with a mean beat frequency of 6 Hz and length of 30 μm, consistent with previous measurements.[1] These cilia create flow speeds of up to 300 μm/s tangential to the surface (and negligible flow through the surface), but which vary in magnitude and direction across the organism—giving rise to the observed vortices. Surprisingly, we observe unusual arrangements of the cilia wherever the surface beat direction reverses (Fig. 2), which we term "defects" by analogy to topological defects observed in nematics and magnetic spins.[11] Cilia beating towards (away from) each other create outwards (inwards) flows and a characteristic tangle (splay) defect, hereafter denoted by + (–) (Supplementary Video 5; 25 larvae). The near-field streamlines match the predicted flow along a wall with a prescribed tangential flow velocity that undergoes a

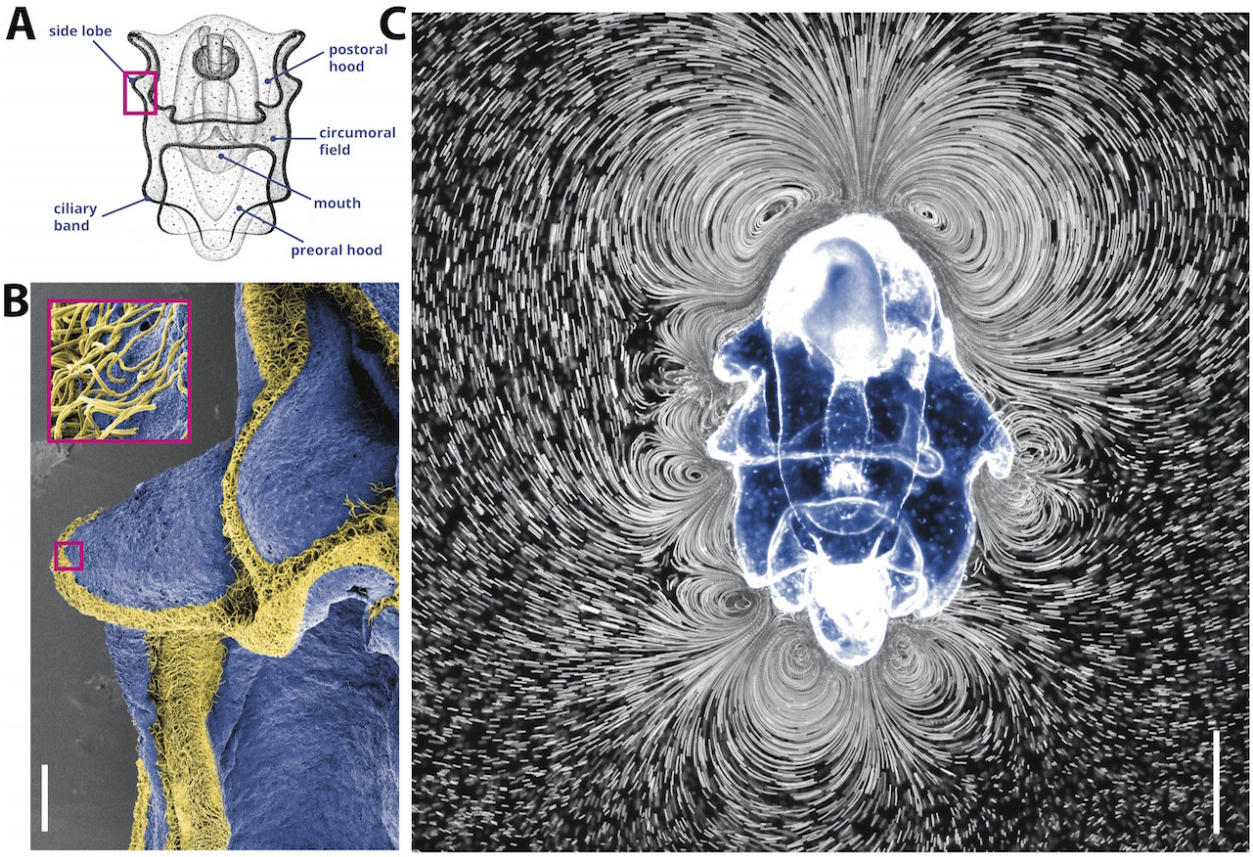

Figure 1 Bat star larvae generate complex arrays of vortices. (**A**) The frontal plane anatomy of a starfish larva, with the ciliary band highlighted as a dark line (adapted from a lithograph by A. Agassiz, 1877). (**B**) A false-color SEM highlighting the ciliary band (yellow). Scale bar: 20 μm. (**C**) An eight-week-old larva feeds even when held captive in a ~ 0.5 mm gap between a glass slide and coverslip. Immobilization enables visualization of 9 counter-rotating vortices by stacking a 3 s dark-field video of 6 μm tracer particles. Scale bar: 350 μm

sudden change in sign (Fig. 2B). We image the defects and flow fields simultaneously, and we observe that each defect creates a boundary between two vortices of opposite rotation direction (Fig. 2C, Supplementary Video 6). Consistent with the time-varying nature of larval swimming, defects can be seen to break up and re-form in place over timescales $\sim$10 s (Fig. 2E, Supplementary Videos 7, 8), creating corresponding changes in the vortices. The defect locations appear to be determined physiologically, and typical locations for a larva are indicated in Figure 2F.

When motile algae (*Rhodomonas lens*, $\sim$ 6 μm) are added to seawater containing 0.75 μm beads, they appear to swim freely until they enter a high-speed ($\sim$ 100 μm/s) region near the body, where they are entrained and repeatedly swept towards the animal's surface by surrounding vortices (Fig. 3A, Supplementary Video 9). Upon approach to the body they may be captured through instantaneous reverse beats of single cilia (Fig. 3B, Supplementary Video 10). This direct-capture mechanism has been reported in other marine plankton—including starfish—as a manifestation of "interception feeding".[5, 8, 12] Hydrodynamically, vortex-mediated surface capture occurs due to short portions of the ciliary band beating in reverse relative to the direction of the prevailing swimming current, which induces recirculation that traps particles near the surface. These regions of the ciliary band span the region between two defects of opposite sign (Fig. 3C). The local structure of this mechanism is consistent across multiple animals; velocity line traces through the vortices overlap when rescaled by vortex speed and size (Fig. 3D), consistent with the power-law scaling expected for a vortex.[11] The velocity drops off with a characteristic $1/r^2$ decay (Fig. 3D), as observed in other systems of confined active swimmers.[13, 14]

We incorporate these observations into a simple mathematical model that captures the tradeoff between near-field feeding and the far-field swimming currents, which are both fully determined by the boundary condition imposed at the larvae's surface. The flows are dominated by viscous rather than inertial forces ($Re < 0.003$), and so we adapt the classic "squirmer" model for the propulsive currents generated by a two-dimensional, circular swim-

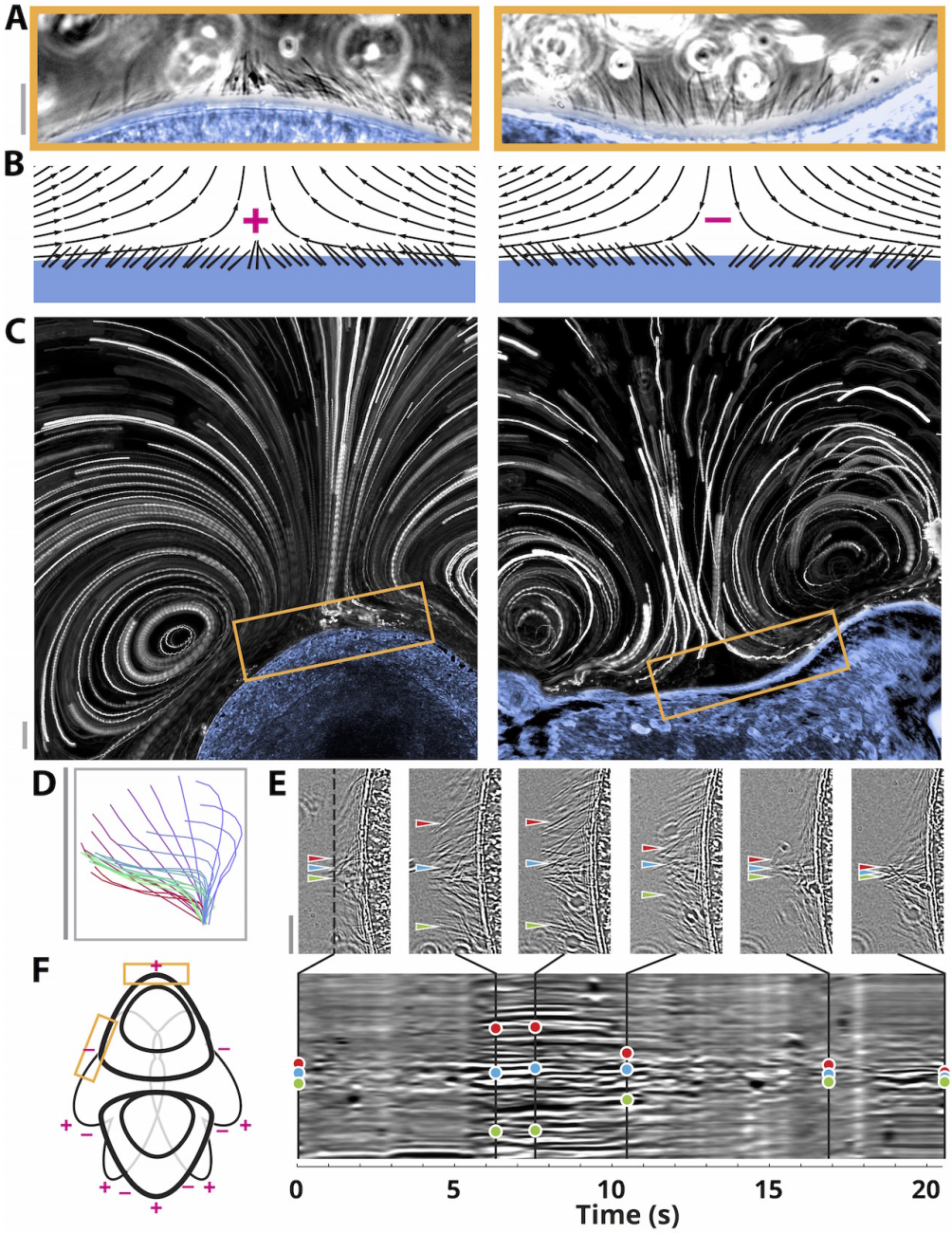

Figure 2 Transient ciliary defects underly vortex formation. (**A**) Boundaries between vortices require local reversals in the surface beat direction of cilia, which create tangles (left, +) or splays (right, –) depending on the rotation directions of the vortices. (**B**) Streamlines for a model flow generated by a sign change in the tangential velocity imposed on a surface, with the orientation of the cilia indicated schematically. (**C**) Zoomed out view of the same video shown in (**A**), with frames stacked over 4.5 s to show pathlines of advected particles near the defect. (**D**) A trace of a typical ciliary stroke near a defect. (**E**) A kymograph of a tangle defect (with the locations of three representative cilia marked) with six video frames called out. (**F**) The locations of + and – defects on a typical larvae, with the locations in the previous panels indicated. Scale bars: 30 μm.

mer imposing an arbitrary tangential velocity profile along its surface—here representing the ciliary band outlining the frontal plane.[15]

$$v_r(r,\theta) = \frac{1}{2}B_1\cos\theta\left(\left(\frac{a}{r}\right)^2 - 1\right) + \sum_{n=2}^{\infty}\frac{n}{2}B_n\cos(n\theta)\left(\left(\frac{a}{r}\right)^{n+1} - \left(\frac{a}{r}\right)^{n-1}\right)$$
$$v_\theta(r,\theta) = \frac{1}{2}B_1\sin\theta\left(\left(\frac{a}{r}\right)^2 + 1\right) + \sum_{n=2}^{\infty}\frac{1}{2}B_n\sin(n\theta)\left(n\left(\frac{a}{r}\right)^{n+1} - (n-2)\left(\frac{a}{r}\right)^{n-1}\right) \quad (1)$$

Where v_r, v_θ denote the radial and azimuthal velocity components in the co-moving frame. Locomotion requires $B_1 \neq 0$ because all terms dependent on r vanish as $r \to \infty$. The squirmer model has been successfully applied to single-celled organisms with localized thrust-generating appendages, which create "pusher/puller" currents that manifest as a single pair of vortices at the fore/aft of the animal.[9, 10] To our knowledge, ours is the first living system in which more than two such vortices are present, and so we introduce higher-order "squirming" terms ($B_n > 0; n > 2$)—which we attribute to the more complex neurociliary control found in invertebrate larvae.[1, 4]

We restrict ourselves to a set of "two-mode" swimmers, each comprising a superposition of a swimming mode (B_1) that generates net propulsion via a streaming flow past the surface, and an "n^{th} order" mode ($B_n, n \geq 2$) that has $2n$ sign changes (ciliary defects) along the surface that generate reversal regions (forming $2n-2$ vortices for $n < 5$, $2n$ vortices for $n \geq 5$). Higher values of n result in smaller average distances between defects of opposite sign. Squirmers with different n are normalized by the maximum surface cilia beat speed and the size of the vortex region (See Supplementary Methods). Streamlines for $n = 1, 3, 4$ are shown in Figure 3E, and the corresponding swimming speeds are observed to decrease with n (Fig. 3F, violet trace).

In order to compare feeding ability for squirmers of different n, we simulate the trajectory of a line source of particles incident on the squirmer, and probabilistically capture particles that pass within a fixed "interception distance" of the surface with a fixed rate per unit time. Example trajectories are shown in Figure 3G, with those of captured particles

highlighted in red. The number of captured particles is rescaled by the initial number of particles, the squirmer diameter, and the interception distance, in order to produce a non-dimensional "capture efficiency" which increases with increasing number of vortices (Fig. 3F, Supplementary Methods). This capture efficiency is comparable to the two-dimensional capture cross-section studied in other model swimmers,[16] and it supports prior experimental observations[1, 6] that longer ciliary bands create a larger volumetric particle "clearance rate." The increased capture efficiency of additional vortices arises purely geometrically, due to a combination of particles slowing and taking repeated passes near the surface—as observed in larval feeding experiments.[6] Adding random noise to the simulated particle trajectories strengthens the observed tradeoff.

Our simple model suggests a plausible reason for the striking flow fields observed around starfish larvae, for which additional vortices increase feeding ability at the expense of swimming speed. This tradeoff is also consistent with the constraints of a fixed energy budget, since the swimmer either dissipates energy due to surface drag from swimming, or vortex core drag from feeding.[11, 15] While previous theoretical studies of feeding vs. swimming in the context of osmotrophic feeders found that the first order swimming mode optimized both swimming and feeding rates,[13, 16, 17] our results support previous evidence that organisms with finite interception/capture rates should favor recirculation currents that slow particles near the surface.[12]

Next we investigate the temporal dynamics of the observed larval flow fields. Figure 4A shows three snapshots of the time-varying flow field around the organism, which changes dramatically over $\sim$10 s timescales (Supplementary Video 11)—representing a known "arresting" behavior of starfish and other larvae in which short pauses punctuate regular swimming[4, 18] (Supplementary Videos 2, 3). In order to quantify these flow field changes, particle image velocimetry (PIV) was used to extract the velocity field as a function of time (Supplementary Methods). Principal component analysis (PCA) was performed on the velocity field time series, resulting in two principal components corresponding to distinct far-field swim-

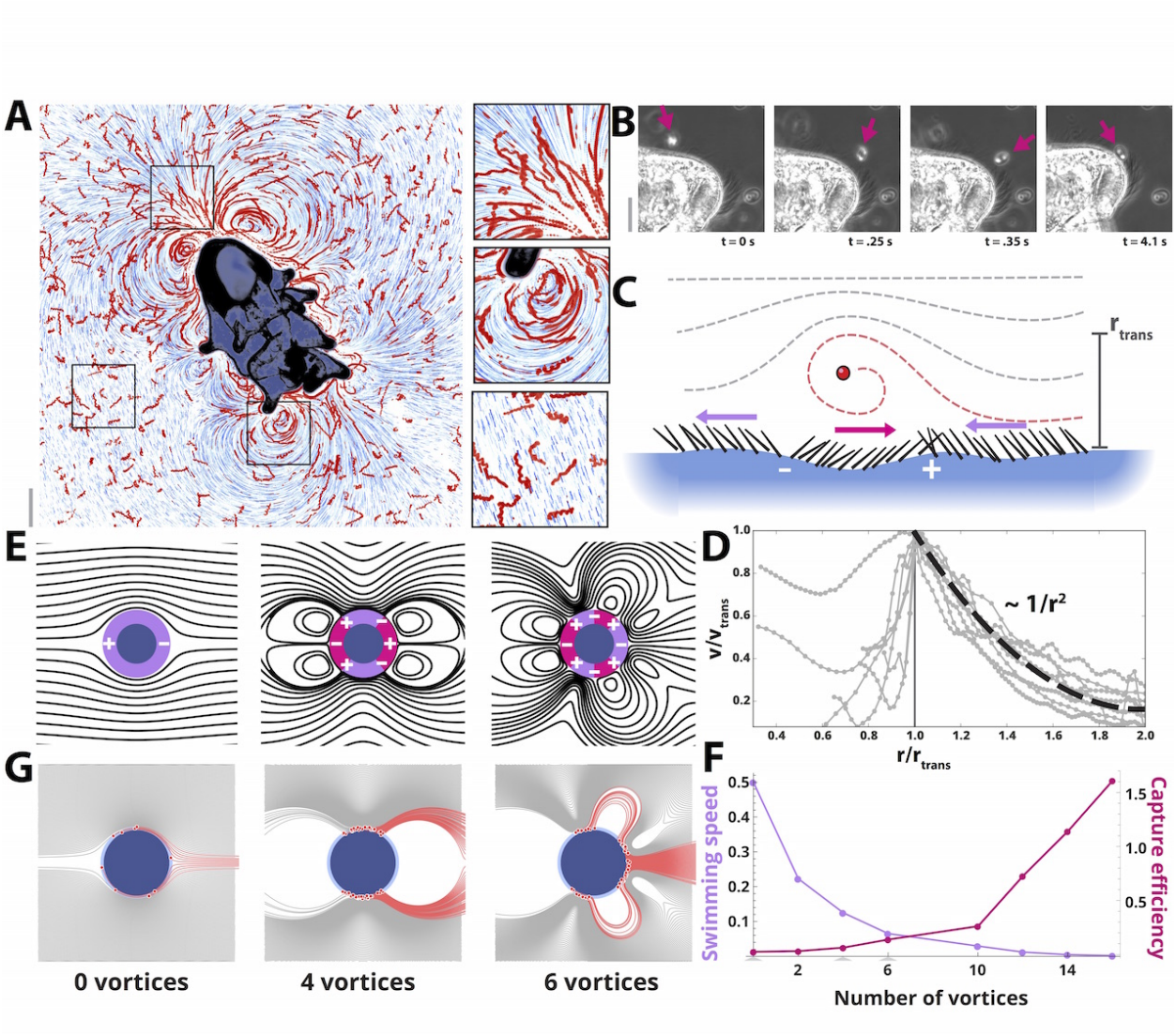

Figure 3 Vorticity arises due to a tradeoff between feeding and swimming currents. (**A**) The flow field generated by a larvae (blue) in a mixture of passive beads (light blue) and active algae (red). Video frames stacked over 60 s, scale bar: 300 μm. (**B**) A typical algae capture sequence, with the algae orientation indicated with an arrow. Scale bar: 40 μm. (**C**) A schematic of flow-induced particle-trapping due to local ciliary reversal between two defects. (**D**) Line traces of the velocity component parallel to the body surface, taken through the largest vortex for 8 organisms (a parabola is overlaid on the decay portions). Streamlines (**E**) and trajectories of incident algae particles (**G**)) for the "two-mode" squirmer for different orders n. Swimming (purple) and reversal (magenta) ciliary regions are indicated, and captured particle trajectories are highlighted in red. (**F**) The swimming speed (purple) and capture efficiency (magenta) as a function of the number of vortices

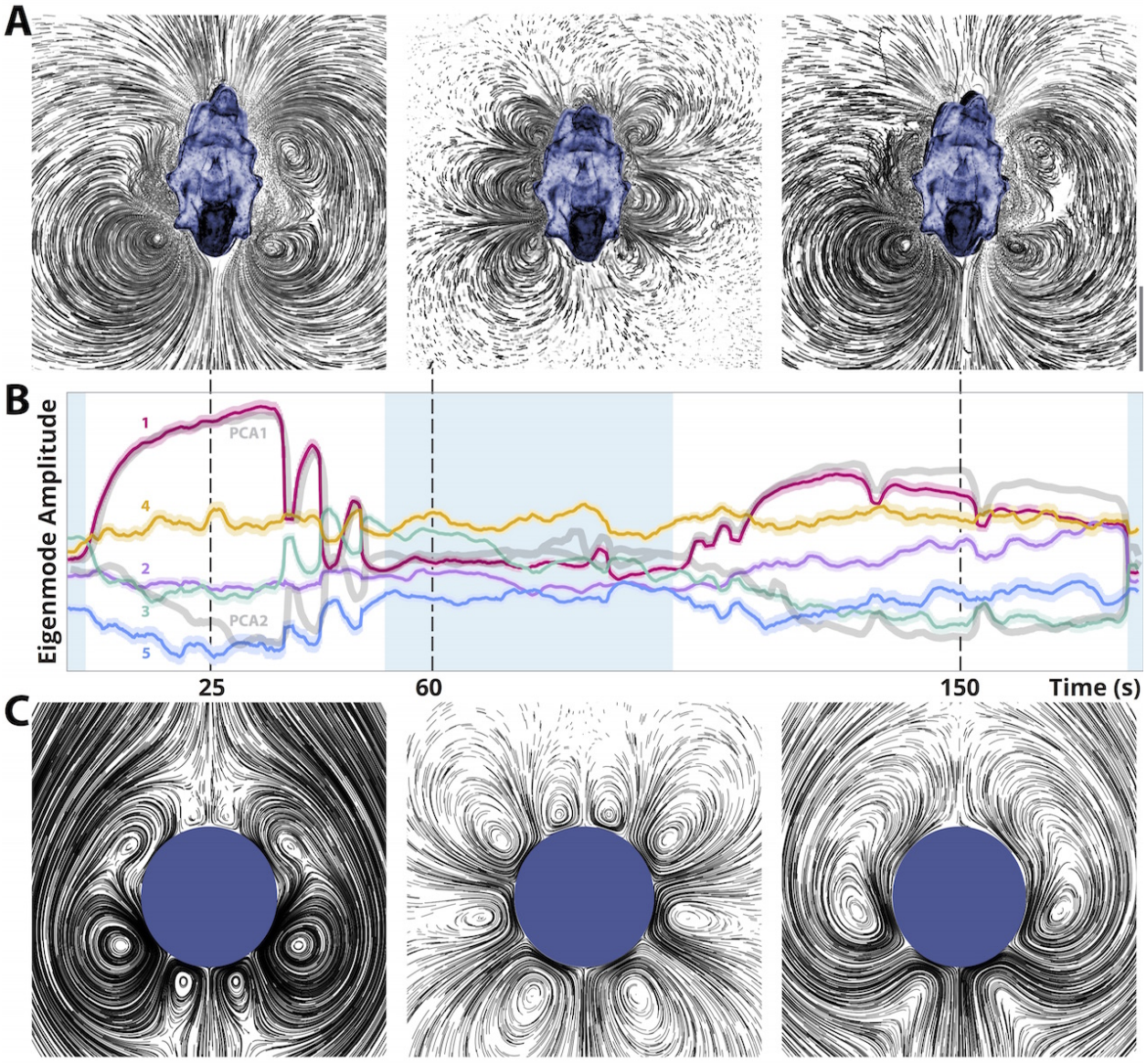

Figure 4 Time-dependent feeding versus swimming behavioral switches. (**A.**) The flow fields generated by an eight-week-old larvae at three different timepoints in a three minute video (Pathline length: 9 s, Scale bar: 500 μm). (**B.**) The relative amplitudes of the first five terms of a least-squares fit of the squirmer model to each frame of the video, with fitting errors shaded. The first-order "swimming" mode corresponds to the magenta trace. The amplitudes of data projections onto the first two principal components are underlaid in gray. Blue boxes underlaid indicate when swimming or feeding dominate in the original video. (**C.**) Simulated particle trajectories for the best-fit squirmer model of the three movie frames shown in (A).

ming and near-field feeding vortex behaviors. Projecting each frame of the PIV data onto the two principal components reveals that the animal switches back and forth between the two modes (Figure 4B, gray traces), consistent with the transitions seen in freely-swimming animals.[4] Direct fitting to the individual modes of the squirmer model (Fig. 4B, colored traces) confirmed that the two anti-correlated principal components correspond to feeding and swimming: the first-order swimming mode (magenta trace) matches the first principal component, while the next four non-swimming modes resemble the anti-correlated component. Plots of the velocity field corresponding to the best fit squirmer model (Fig. 4C) qualitatively resemble the original movie frames (Fig. 4A).

The correspondence of the PCA and squirmer fits suggests that the larval behavior is dominated by characteristic "eigenstrokes"—feeding and swimming—that can be represented as amplitudes of a finite set of coefficients in the squirmer model. Low-dimensional behavior has been observed in other living systems[19–21] however, ours is the first in which these characteristic behaviors can be directly linked with both the governing physical equations (Stokes' flow) and opposing biological functions (feeding and swimming). This behavioral switching may represent an adaptive strategy for heterogenous environments, analogous to the "roaming/dwelling" transition observed in other organisms that constitutes an optimal trade-off between global exploration and local exploitation.[22]

The complex spatiotemporal properties of the starfish larval flow field extend earlier results suggesting that the feeding/swimming dichotomy may be a fundamental design principle for marine invertebrate larvae.[12, 18, 23] Previously-identified neurociliary control mechanisms in invertebrate larvae,[4, 24] coupled with fluid dynamics, may link behavior, adaptation, and morphology through the mechanics of the ciliary band.[1, 5, 6] In particular, our observed ciliary defects may originate in the finite axonal contact range of the neurons responsible for ciliary control in many invertebrate larvae.[25] As a result, our findings may have implications for pathologies involving collective ciliary dyskinesia.[26] Moreover, it may be possible to implement "driven defect" boundary conditions in artificial systems as a means of stably

generating complex flow structures,[27] with applications to soft robotics and impingement filtration.

1 Acknowledgments

We thank C. Lowe, D. N. Clarke, K. Uhlinger, and Stanford BIOS 236; also M. S. Bull, D. Krishnamurthy, L.-M. Joubert, and the Prakash Lab. This work was supported by an ARO MURI Grant W911NF-15-1-0358 and an NSF CAREER Award (to M.P.) and an NSF GRFP DGE-114747 (to W.G.)

References

[1] Strathmann, R. R. The feeding behavior of planktotrophic echinoderm larvae: mechanisms, regulation, and rates of suspension feeding. *Journal of Experimental Marine Biology and Ecology* **6**, 109–160 (1971).

[2] Nielsen, C. Structure and function of metazoan ciliary bands and their phylogenetic significance. *Acta zoologica* **68**, 205–262 (1987).

[3] Strathmann, R. R. Hypotheses on the origins of marine larvae. *Annual Review of Ecology and Systematics* 89–117 (1993).

[4] Lacalli, T., Gilmour, T. & West, J. Ciliary band innervation in the bipinnaria larva of Piaster ochraceus. *Philosophical Transactions of the Royal Society of London B: Biological Sciences* **330**, 371–390 (1990).

[5] von Dassow, G., Emlet, R. B. & Maslakova, S. A. How the pilidium larva feeds. *Frontiers in zoology* **10**, 1 (2013).

[6] Hart, M. W. Particle captures and the method of suspension feeding by echinoderm larvae. *The Biological Bulletin* **180**, 12–27 (1991).

[7] Agassiz, Alexander. *North American starfishes*, vol. 5 (Welch, Bigelow, and Company, University Press, 1877).

[8] Strathmann, R. R. Larval feeding in echinoderms. *American zoologist* **15**, 717–730 (1975).

[9] Goldstein, R. E. Green algae as model organisms for biological fluid dynamics. *Annual review of fluid mechanics* **47**, 343 (2015).

[10] Guasto, J. S., Rusconi, R. & Stocker, R. Fluid mechanics of planktonic microorganisms. *Annual Review of Fluid Mechanics* **44**, 373–400 (2012).

[11] Chaikin, P. M. & Lubensky, T. C. *Principles of condensed matter physics*, vol. 1 (Cambridge Univ Press, 2000).

[12] Kiørboe, T. How zooplankton feed: mechanisms, traits and trade-offs. *Biological Reviews* **86**, 311–339 (2011).

[13] Magar, V., Goto, T. & Pedley, T. Nutrient uptake by a self-propelled steady squirmer. *The Quarterly Journal of Mechanics and Applied Mathematics* **56**, 65–91 (2003).

[14] Pepper, R. E., Roper, M., Ryu, S., Matsudaira, P. & Stone, H. A. Nearby boundaries create eddies near microscopic filter feeders. *Journal of The Royal Society Interface* rsif20090419 (2009).

[15] Blake, J. Self propulsion due to oscillations on the surface of a cylinder at low Reynolds number. *Bulletin of the Australian Mathematical Society* **5**, 255–264 (1971).

[16] Tam, D. & Hosoi, A. Optimal feeding and swimming gaits of biflagellated organisms. *Proceedings of the National Academy of Sciences* **108**, 1001–1006 (2011).

[17] Michelin, S. & Lauga, E. Optimal feeding is optimal swimming for all Péclet numbers. *Physics of Fluids (1994-present)* **23**, 101901 (2011).

[18] Strathmann, R. R. & Grünbaum, D. Good eaters, poor swimmers: compromises in larval form. *Integrative and Comparative Biology* **46**, 312–322 (2006).

[19] Berman, G. J., Choi, D. M., Bialek, W. & Shaevitz, J. W. Mapping the stereotyped behaviour of freely moving fruit flies. *Journal of The Royal Society Interface* **11**, 20140672 (2014).

[20] Stephens, G. J., Johnson-Kerner, B., Bialek, W. & Ryu, W. S. Dimensionality and dynamics in the behavior of C. elegans. *PLoS Comput Biol* **4**, e1000028 (2008).

[21] Jordan, D., Kuehn, S., Katifori, E. & Leibler, S. Behavioral diversity in microbes and low-dimensional phenotypic spaces. *Proceedings of the National Academy of Sciences* **110**, 14018–14023 (2013).

[22] Berg, H. C. *Random walks in biology* (Princeton University Press, 1993).

[23] Malkiel, E., Sheng, J., Katz, J. & Strickler, J. R. The three-dimensional flow field generated by a feeding calanoid copepod measured using digital holography. *Journal of Experimental Biology* **206**, 3657–3666 (2003).

[24] Iwadate, Y. & Suzaki, T. Ciliary reorientation is evoked by a rise in calcium level over the entire cilium. *Cell motility and the cytoskeleton* **57**, 197–206 (2004).

[25] Jékely, G. Origin and early evolution of neural circuits for the control of ciliary locomotion. *Proceedings of the Royal Society of London B: Biological Sciences* **278**, 914–922 (2011).

[26] Marshall, W. F. & Kintner, C. Cilia orientation and the fluid mechanics of development. *Current opinion in cell biology* **20**, 48–52 (2008).

[27] Shields, A. *et al.* Biomimetic cilia arrays generate simultaneous pumping and mixing regimes. *Proceedings of the National Academy of Sciences* **107**, 15670–15675 (2010).